Available online at www.sciencedirect.com
SCIENCE DIRECT®
Journal of Electroanalytical Chemistry 554–555 (2003) 133–143
Journal of Electroanalytical Chemistry
www.elsevier.com/locate/jelechem

The influence of the surface electric field on water ionization: a two step dissociative ionization and desorption mechanism for water ion cluster emission from a platinum field emitter tip

Christopher J. Rothfuss, Valentin K. Medvedev, Eric M. Stuve *

Department of Chemical Engineering, University of Washington, Box 351750, Seattle, WA 98195-1750, USA

Received 3 October 2002; received in revised form 15 January 2003; accepted 6 February 2003

Abstract

Water ionization and desorption of protonated water clusters in high electric fields were studied on a Pt emitter tip in ultrahigh vacuum. Ramped field desorption (RFD) experiments were carried out at 109 and 145 K. As the tip potential was linearly ramped, crystalline ice adsorbed at low temperatures (145 K) was ionized and emitted from the tip as protonated water clusters $H^+(H_2O)_n$. Emitted ions were mass resolved using a Wien filter for n up to 7. The onset of ionization occurred at a higher field for the 109 K RFDs (0.44 V $Å^{-1}$) than for the 145 K RFDs (0.32 V $Å^{-1}$). All observed ions for each temperature were observed simultaneously in the onset flash. However, clusters $n = 2$ and 3, which were dominant at 109 K, were not observed at 145 K. These results, coupled with previous low temperature (109–150 K) ice field desorption data, and higher temperature (170–300 K) field adsorbed ion emission data, suggest a two step dissociative ionization/desorption mechanism in which the strongly temperature dependent, dissociative ionization event determines emission onset at low temperatures, while the field dependent, ion emission event determines emission onset at higher temperatures. In addition, local enhancement of the ionization event was observed by directly imaging ion cluster emission using field ion microscopy.
© 2003 Elsevier Science B.V. All rights reserved.

Keywords: Desorption; Electric field; Solvation; Deprotonation

1. Introduction

One of the features inherent to a metal surface is the presence of a strong electrical field. This field naturally arises as a result of the change in electron density between the Fermi level of the metal and its surrounding medium, whether vacuum or solution. Since the change in electron density occurs over a distance of a few angstroms, and typical potential differences between the Fermi and vacuum levels (i.e., the work function) are several electron-volts, it is straightforward to estimate that surface electric fields must be on the order of 1 V $Å^{-1}$ (100 MV cm^{-1}). While truly colossal, such fields are not generally studied explicitly because they follow from the change in electron density at the interface. Thus, any unusual property of the surface, for example the catalytic property of platinum, already follows from the presence and specific nature of the surface field.

In the electrochemical context, however, the nature and influence of the surface electric field takes on an exciting and important role. Because the electrode potential can be easily controlled, whether by charging the electrode from an external source or by chemically pinning its Fermi level (as in electrocatalytic fuel cell reactions), the magnitude of the surface electric field can be altered also on the order of 1 V $Å^{-1}$. That is, the surface electric field can be changed on the same order of its naturally occurring value, even to an extent that reverses its sign! Of course, such behavior lies at the heart of electrochemistry itself and the ability of electrode | electrolyte interfaces to make and break chemical bonds.

Understanding the role of surface electric fields in electrochemistry has been of theoretical interest for a

* Corresponding author. Tel.: +1-206-543-2250; fax: +1-206-543-3778.
E-mail address: stuve@u.washington.edu (E.M. Stuve).

0022-0728/03/$ - see front matter © 2003 Elsevier Science B.V. All rights reserved.
doi:10.1016/S0022-0728(03)00131-1

number of years; for some representative work see Refs. [1–3]. However, experimental studies of the role of surface electric fields are quite few, due in large part to the difficulty of generating such high fields in a reproducible fashion. With planar electrodes, for example, a field of 1 V Å^{-1} would require a potential difference of 10 000 V across two electrodes spaced 1 μm apart. Even if the dielectric medium between the two electrodes could withstand such a field (or one had a perfect vacuum), the force due to coulombic attraction of the two electrodes would be on the order of 5000 atm, essentially guaranteeing that the electrodes would collapse upon themselves regardless of their supports.

Instead, the methodology of ultrahigh vacuum (UHV) double layer modeling was developed to provide information about electrode | electrolyte interface phenomena [4,5]. This methodology consists of adsorbing relevant electrochemical species on a metal substrate in vacuum to mimic the electrode | electrolyte interface. A number of publications have shown the close relationship of these experiments in simulating the charging of an electrode surface [6–8].

These early efforts in electrochemical simulation did not take on the issue of surface electric fields directly, however. Beginning in the early 1990s Mike Weaver and his coworkers took advantage of the sensitivity of the stretching frequency of adsorbed CO to changes in the electric field (the Stark tuning effect) to begin an extensive inquiry into the role of the surface electric field and the relationship between real electrochemical and UHV double layer modeling experiments. This work combined vacuum and electrochemical measurements of CO vibrational spectra with vacuum measurements of work function conducted in a large variety of solvents and computational studies in collaboration with Marc Koper. A large number of papers appeared on this topic, among the most significant being Refs. [9–14]. Some of the new findings from this work include (1) demonstration of the solvation effect of water on adsorbed CO in the absence of an applied field, i.e. at the potential of zero charge [9], (2) the use of coadsorbed alkali ions to effect substrate charging in vacuum and demonstration of the equivalence of such systems with potential-dependent, electrochemical vibrational measurements [10], (3) that most of the interfacial potential drop occurs across the adsorbed CO adlayer and is relatively insensitive to solvent [10], (4) that the quality of agreement between electrochemical and UHV vibrational spectra of CO and NO can be used to estimate the so-called absolute electrode potential [11], (5) that there is little difference between local and average electric fields for both the cases of adsorbed CO and NO [12], and (6) a comprehensive analysis of field-effects on metal-adsorbate bonding and Stark tuning shifts [13,14]. In particular, the strength of metal-adsorbate bonding is determined by the static dipole moment, whereas the Stark tuning shift is determined by the dynamic dipole moment.

During the same period our research group undertook a different approach to experimental studies of the surface electric field. To circumvent the problems of planar electrodes we adopted the field emitter tip configuration, whereby sufficiently high electric fields can be obtained by field concentration at a sharp tip ($\sim$300 Å radius) biased at several 1000 V. This configuration enables essentially arbitrarily high electric fields to be produced, limited only by the ability of the tip to withstand the applied fields. In these experiments we probe field-ionization of water to form hydrated protons and hydrated hydroxide ions, one of the most fundamental of electrochemical reactions. In so doing we hope to achieve an understanding of how water behaves in the surface electric field, in terms of solvation, dielectric screening, and reaction—information complementing that obtained by Weaver's research of the last 10 years.

The study of water on a field emitter tip dates back to 1955 when Inghram and Gomer [15] observed the formation of ion clusters on a tungsten tip. Beckey [16] further characterized water ionization by identifying the emitted ions as protonated water clusters of varying size. Schmidt [17] later provided critical ionization potentials for water on tungsten, iridium and platinum. Anway [18] extended field-ionization experiments to field adsorbed water layers at room temperature. More recently, Stintz and Panitz have studied both protonated water clusters [19,20] and negative ion water clusters [21] using a technique called ramped field desorption (RFD) and characterized the sizes of the ion clusters produced as the emitter tip field was ramped. Recent work by our group [22–26] has probed the onset of ionization of these water clusters from a Pt emitter tip as a function of the adsorbed layer thickness and tip temperature in an effort to investigate the mechanism of ionization and the response of the nearby, non-reactive water molecules. Additionally, molecular dynamics studies and ab initio calculations have attempted to quantify dissociation probabilities for water [27], as well as solvation energies [28,29], solvation dynamics [30], and local electric fields [31] present in liquid water and ice.

Our recent investigations [26] into the temperature and field dependence of protonated water cluster emission from water adlayers on Pt have provided an understanding of the cluster emission behavior. A protonated water cluster may form on the surface through dissociative ionization of a water molecule according to

$$m\mathrm{H_2O} \rightarrow \mathrm{H^+(H_2O)}_n + \mathrm{OH^-(H_2O)}_{m-n-1} \quad (1)$$

A protonated water cluster residing on the surface has essentially three available pathways. The first possibility is emission,

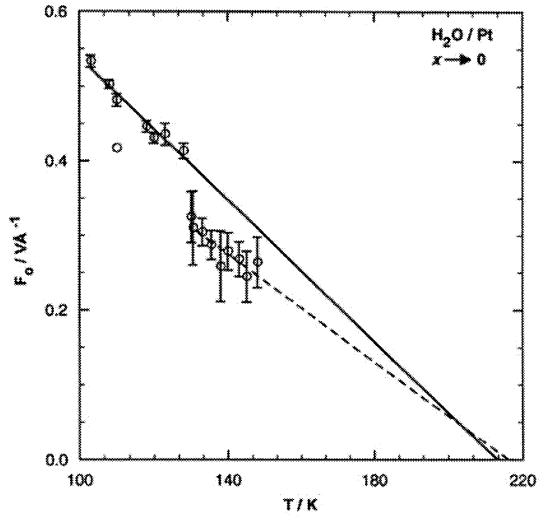

(a)

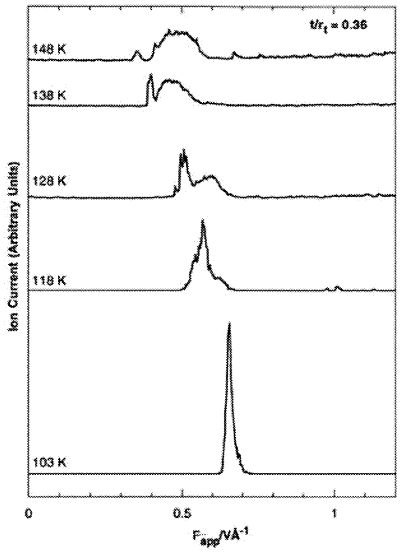

(b)

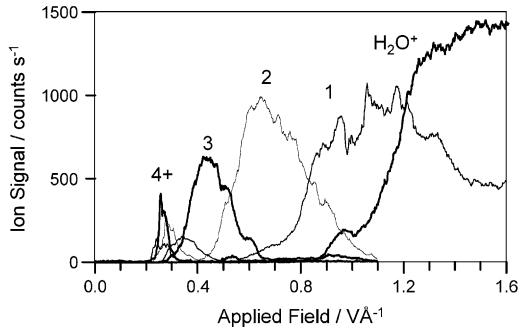

(c)

$$H^+(H_2O)_n \rightarrow H^+(H_2O)^*_{m\leqslant n} + (n-m)H_2O \quad (2)$$

where n represents the number of water molecules solvating the proton on the surface and m represents the number of water molecules in the emitted ion cluster, which is designated by an asterisk. Emission is a strongly field dependent phenomenon and largely independent of temperature. This independence logically follows from a comparison of the emission energies (typically about 4 eV), and the thermal energy of the tip (~ 0.02 eV). Calculated emission energies [26] showed a dependence of emission barrier on cluster size in which large clusters are more easily emitted than are small clusters, consistent with the experimental field dependence of ion emission.

The second possibility for the solvated water cluster residing on the tip surface is to associate with an additional surface adsorbed water molecule,

$$H^+(H_2O)_n + H_2O \rightarrow H^+(H_2O)_{n+1} \quad (3)$$

if another molecule is locally available. This provides additional solvation energy, and proceeds readily at the limit of availability.

The third possibility is thermal desorption of the nth solvating molecule,

$$H^+(H_2O)_n \rightarrow H^+(H_2O)_{n-1} + H_2O^* \quad (4)$$

This pathway is thermally activated and almost completely field independent. The nth water molecule is bound to the proton by the solvation energy associated with the transition from $H^+(H_2O)_n$ to $H^+(H_2O)_{n-1}$. With increasing temperature, the extent of solvation of the proton diminishes, and emission of large ion clusters becomes impossible. So it was concluded from our studies that for temperatures from 170 to 300 K, the dominant ion emission clusters were determined by the applied field from a set of possible cluster types, which was determined by the tip temperature.

Pinkerton and coworkers [22–25] investigated ionization thresholds for protonated water clusters using RFD. For crystalline ice deposited at 145 K and in the limit of zero thickness, they reported a correlation between ionization onset field and tip temperature, with a line break near 130 K and an extrapolated intercept near 210 K (shown in Fig. 1a). The slope break is likely due to the onset of surface diffusion. The

Fig. 1. Previous protonated water cluster emission results. (a) Applied field F_A for ion emission onset as a function of temperature T in the limit of zero coverage for water deposited on a Pt emitter tip. Reprinted from Scovell et al. [24]; (b) RFD total ion current for adsorbed water (ice) layers. Dimensionless ice thickness (thickness water/tip radius) was 0.35. Reprinted from Scovell et al. [24]; (c) mass selected ion current for field desorption of field adsorbed water from a Pt emitter tip at 180 K at a H_2O partial pressure of 5×10^{-6} Torr. Protonated water clusters $H^+(H_2O)_n$ are observed for $n = 1$–$4+$.

intercept corresponds to the field-free ionization temperature for an ice layer of zero thickness. Fig. 1b illustrates the behavior of the ion signal during the field ramp. The ion current showed a sharp onset field and a relatively narrow peak. The results of these earlier RFDs were very different from our recently published field adsorbed experiments above 170 K, an example of which is shown in Fig. 1c. The onset field for ion emission actually increased with increasing temperatures in these field adsorbed experiments, in stark contrast to the extrapolated line shown in the low temperature graph. This contrast in behavior for the RFD of field adsorbed water at temperatures above 170 K and field-free adsorbed ice below 145 K suggests a difference in the limiting step for ion emission between the two cases.

2. Experimental

2.1. Apparatus and procedure

The experimental apparatus and techniques have been described previously in detail and will only be summarized here [26,32]. The UHV chamber, outlined in Fig. 2, was equipped with analytical equipment for performing field ion microscopy (FIM), field emission microscopy, $E \times B$ (Wien filter) and pulsed time of flight ion mass spectrometry, and residual gas analysis. A downtube with emitter tip assembly (Fig. 2e) was mounted onto a polar coordinate manipulator for orientation towards either a micro-channel plate/phosphor screen assembly for ion/electron imaging, or a lens assembly for mass resolved analysis of emitted ions. The lens assembly focused the ion beam towards a Wien filter assembly (Fig. 2c) and drift tube (Fig. 2b). The tip translation apparatus allowed rotation of the tip assembly about the z-axis, translation along the z-axis, and a small degree of angular manipulation from the axis. The tip assembly was mounted on a coldfinger downtube for cooling the apparatus with liquid nitrogen. The chamber was pumped by turbomolecular and titanium sublimation pumps to a base pressure of 10^{-10} Torr.

Platinum emitter tips were prepared by electrochemically etching a 0.13 mm Pt wire in a 500 K mixture of sodium chloride and sodium nitrate [33]. The Pt tip of approximately 350 Å radius and [100] orientation was spot-welded to a 0.25 mm Pt wire heating loop and mounted onto the liquid nitrogen cooled downtube. The cryo-cooled tip, at a base temperature of 105 K, was resistively heated to the desired experimental temperature. The tip temperature was measured with a chromel–alumel thermocouple spot-welded to the heating loop near the tip. The tip potential was controlled with a ± 5 kV power supply. A planar counter electrode with a 5-mm circular hole was positioned coaxialy with the tip apex at a distance of 1 mm. The counter electrode potential was independently regulated to ± 5 kV. The tip/counter electrode configuration provided fields greater than 4 V Å^{-1}, sufficient to field-evaporate Pt and thus clean the tip.

The ion focusing lens was similar to the symmetric, three-electrode, unipotential type suggested by Rempfer [34]. To eliminate aberrant electrical fields, stainless steel cylindrical rings were welded to the entrance and exit electrodes of the lens in its inner part. The lens focused ions through the Wien filter, providing ion signals of around 10^3 counts s^{-1} for a tip of radius 350 Å as configured. The Wien filter employed crossed electric and magnetic fields to select ion mass to charge ratios. The electrical force on the ion is proportional to charge, while the magnetic force is proportional to both charge and ion velocity. By aligning the forces in opposition,

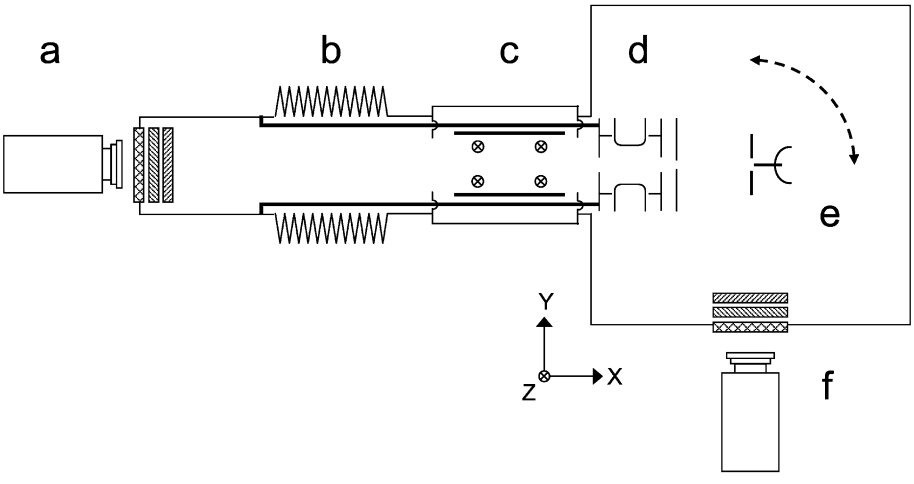

Fig. 2. Schematic of experimental system. (a) Multi-channel plate/phosphor screen assembly with CCD camera for signal measurement and visual focusing of ion signal. (b) Ion flight tube with adjustable bellows. (c) Wien filter ($E \times B$) assembly for mass selection. (d) Lens assembly for ion focusing. (e) Rotatable emitter tip assembly. (f) Multi-channel plate/phosphor screen assembly for direct imaging (FIM).

the fields may be balanced for a given velocity. As a result, only ions with the selected velocity will proceed straight through the crossed fields; all others will have their paths deviated and terminated. By forming all ions at a uniform potential, this velocity selection effectively provides mass to charge selectivity.

The gas handling system for the chamber was independently pumped using a mechanical pump. Gases were introduced through either a needle valve with sensitivity down to 10^{-7} Torr, or a variable leak valve, for control to better than 10^{-8} Torr. The water samples used for dosing were prepared by triply freezing nanopure, de-ionized water to 77 K and evacuating the containment vessel. A final freeze and evacuation of the vessel was performed at 195 K.

Prior to all testing, the Pt emitter tip was field-cleaned and imaged with neon gas. Cleaning was accomplished by field-evaporating a small amount of Pt from the surface while visually inspecting the imaged surface until it appeared atomically clean and structured. Simple annealing of the tip was not sufficient to remove all contaminants from the surfaces, especially carbon. Field-cleaning ensures complete removal of surface contaminants prior to testing and reduces the possibility of undesired surface reactions or interactions.

Two series of tests were conducted to characterize the mechanism of water ion cluster formation in a field adsorbed water layer on the platinum emitter tip. First, the Wien filter was used for mass selecting a particular water cluster ion signal for a series of isothermal ramped field-ionization and desorption experiments. For the second, the Pt tip was directly imaged using water as the imaging gas at 180 and 230 K for a variety of fields.

2.2. Mass selected RFD

After imaging and field-cleaning, the tip potential V_t and counter electrode potential V_{CE} were each set to +3 kV. The cryo-cooled tip was then resistively heated to 145 K for water deposition. Water was deposited at a partial pressure of 2×10^{-7} Torr for 5 min, resulting in a deposition thickness of approximately 100 Å. Under these conditions, water is deposited as crystalline ice [35]. The tip was then heated or cooled to the desired temperature for the field desorption. The Wien filter was tuned to select a particular ion mass. To maintain a constant ion formation potential with respect to ground, the tip potential was held constant while the counter electrode potential was ramped from +3000 to 0 V at a rate of 10 V s^{-1} to increase the local field. The constant ion formation potential is important for both lens focusing and consistent Wien filter results. A computer data acquisition system recorded the mass selected ion signal as a function of potential. After each RFD, the tip potential was taken to the field-cleaning potential at 110 K to refresh the tip. The Wien filter was then tuned to a different mass, water was again adsorbed, and the ramping procedure was repeated. RFDs for each cluster type were performed for n up to 7 at both 109 and 145 K.

2.3. Direct ion imaging

The Pt emitter tip was positioned at the MCP/phosphor screen for direct imaging of ion cluster formation on the tip surface. Prior to imaging with water, the tip was field-cleaned in neon. The tip potential was set to 3 kV and the counter electrode potential was set according to the desired ion cluster formation size as determined from previous experiments. Water was introduced to the chamber to a pressure of 5×10^{-6} Torr. This establishes a steady state ion signal, as opposed to the discrete ion signal of the RFDs. The ion signal from the Pt tip was amplified by the MCPs and the image on the phosphor screen was recorded with a CCD camera. The CCD camera signal was acquired by the computer at a scan rate of 5 frames s^{-1} and resolution of 640×480 pixels. This procedure was repeated for a series of potentials at both 180 and 230 K.

3. Results

Fig. 3 depicts the results of the RFD experiments. The 109 K data in Fig. 3a shows ion signal from all masses $n = 2$–7, with the dominant mass at $n = 3$. The ion emission signals occurred simultaneously (in a flash) at an applied field of 0.44 V $Å^{-1}$. For the higher temperature experiments at 145 K (Fig. 3b), the ion content was changed and the onset occurred at a lower field of 0.32 V $Å^{-1}$. This ramp showed only clusters $n = 4$–7. The dominant $n = 3$ peak observed in the 109 K system was absent at 145 K. Again, all clusters occurred simultaneously at the ionization onset in a flash for a given experiment. The slight onset deviation exhibited between the differing masses is due to the deviations from experiment to experiment.

Fig. 4 illustrates the spatial distribution of ion cluster formation under steady state tip conditions, time-averaged over 10 s, for a variety of potentials at 180 and 230 K. Intense white areas represent localized ion formation throughout the 10 s measurement period. The micrograph in Fig. 4a is the signal average for a tip field favoring large ion cluster formation ($n > 4$; $F = 0.27$ V $Å^{-1}$) at 180 K. Few ion sources were present, but those present persisted for all or most of the imaging time. In Fig. 4b ($n = 4$; $F = 0.34$ V $Å^{-1}$), ion formation occurred from a larger number of sources with similar persistence of signal. Fig. 4c shows conditions ($n = 3$; $F = 0.45$ V $Å^{-1}$) optimal for emission of $n = 3$ clusters. The size and number of localizations again increased. In

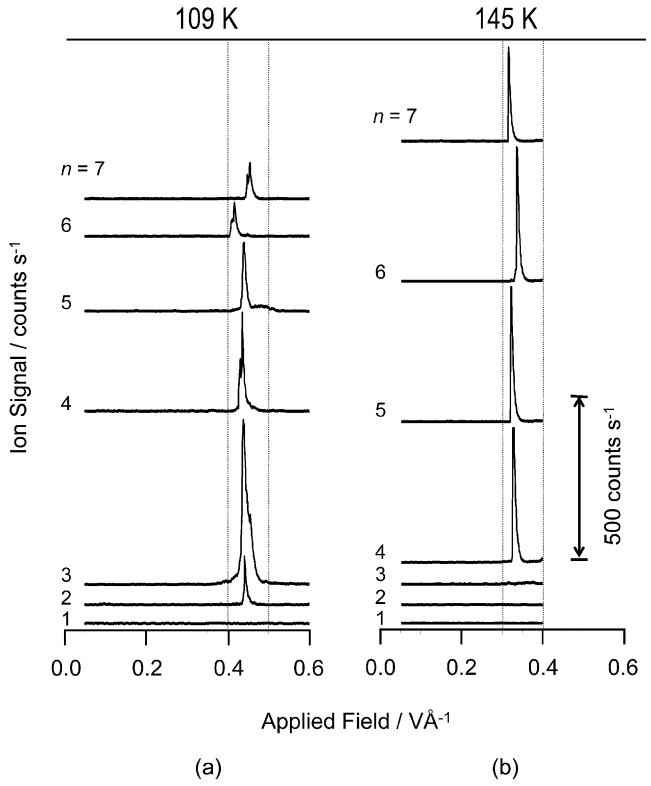

Fig. 3. Mass selected RFD of ice layers from a Pt field emitter tip of radius ~350 Å. Crystalline ice was deposited at 145 K to a thickness of 100 Å. Protonated water clusters $H^+(H_2O)_n$ are shown for n up to 7. (a) Tip cooled to 109 K for RFD. (b) Tip at 145 K for RFD.

Fig. 4d ($n=2$; $F=0.64$ V Å^{-1}), the number of sources increased further, but the intensity of each localization appears less. This trend is more pronounced for the transition from Fig. 4d and e ($n=1$; $F=1.0$ V Å^{-1}). In Fig. 4e, many small localizations remained for the course of the experiment. Additionally, in both Fig. 4d and e there are numerous localizations that did not persist throughout the experiment, which appear as gray spots. Fig. 4f shows the tip at a field (H_2O^+; $F=1.6$ V Å^{-1}) where field-ionization of the water molecules occurs directly, prior to dissociation on the surface. No sustained localizations are visible. Fig. 4g and h were recorded at 230 K for the same fields as Fig. 4d and e, respectively. The increased temperature increases the size of the localizations while decreasing their number. Finally, Fig. 4i is a picture of the platinum tip cleaned and imaged with neon after testing.

4. Discussion

4.1. Mass selected ramped field-ionization and desorption of ice layers

The emission mechanism outlined previously [26] provides an understanding of the behavior of the emission for the field-adsorbed system (i.e. at higher temperature), but does not explain the low temperature RFDs. At low temperatures adsorbed ice layers provide sufficient water coverage for large cluster emission, but fail to emit clusters until higher fields. It is also important to note that the apparent emission barrier determined by Scovell et al. was ~0.7 eV, which is nearly equal to the activation energy for molecular dissociation of bulk water [24], suggesting that under their experimental conditions, ion emission was determined by the onset of dissociative ionization. While the dissociation event is strongly field dependent, it is much more strongly influenced by temperature than the emission barriers observed for the higher temperature work in the field adsorbed water layers. This is because the activation barrier for dissociation is significantly lower than the field-free barrier for ion emission (~4 eV).

Based on the field-adsorbed ion emission results coupled with the low temperature RFD data, it appeared that dissociative ionization was rate limiting at low temperatures while cluster emission was rate limiting at higher temperatures in determining ion current. Therefore, another line of experiments was performed to test this hypothesis. The same RFD experiments performed by Pinkerton and coworkers [22–25] at low temperatures were repeated at 109 and 145 K, but with mass resolved ion analysis, as shown in Fig. 3. The procedure for these experiments was the same as that used for field adsorbed RFD with the exception of the dosing technique.

The behavior of these mass resolved low temperature RFDs supports the two-step hypothesis where dissociative ionization and ion emission occur as separate events. The same field dependent emission barriers observed in the high temperature work still hold at low temperatures for determining which cluster types are energetically accessible for emission. The difference is that at these low temperatures the field ramp passes through several emission barriers prior to reaching the dissociation barrier. This behavior can be illustrated by considering the three ramps shown in Fig. 5. For this figure, the dissociation line is taken from Ref. [24], while the cluster emission fields (horizontal lines) are taken from previous field adsorbed RFD experiments [26]. In RFD1 (109 K), the ramped field passes through the emission field for each cluster, beginning with the high masses and moving in turn through $n=2$, immediately prior to intersecting the dissociation barrier. Upon reaching the dissociation field, ion emission begins in a flash containing all of the cluster types beneath the dissociation line. As observed with the ion population shown in Fig. 3a, all ion clusters $n>1$ are energetically accessible when the dissociation event occurs. However, the $n=2$ cluster is barely accessible so the primary cluster type remains $n=3$. For RFD2 (145 K), the field

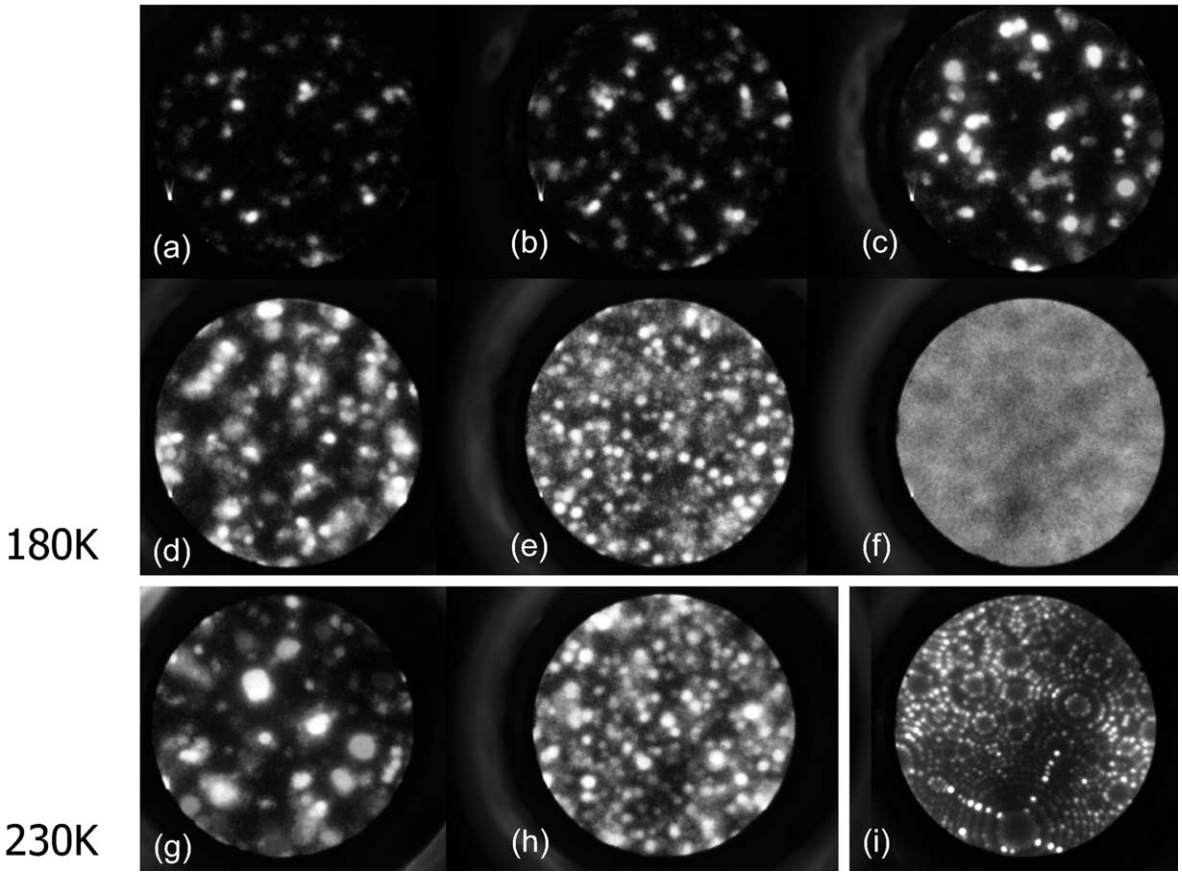

Fig. 4. Field ion micrographs of protonated water cluster $H^+(H_2O)_n$ emission at 180 and 230 K for a variety of fields selected for favoring particular clusters types. Micrographs represent 10 s of signal averaged ion intensity. (a) Clusters $n > 4$; $F = 0.27$ V Å^{-1}; $T = 180$ K. (b) Cluster $n = 4$; $F = 0.34$ V Å^{-1}; $T = 180$ K. (c) Cluster $n = 3$; $F = 0.45$ V Å^{-1}; $T = 180$ K. (d) Cluster $n = 2$; $F = 0.64$ V Å^{-1}; $T = 180$ K. (e) Cluster $n = 1$; $F = 1.0$ V Å^{-1}; $T = 180$ K. (f) H_2O^+; $F = 1.6$ V Å^{-1}; $T = 180$ K. (g) Cluster $n = 2$; $F = 0.64$ V Å^{-1}; $T = 230$ K. (h) Cluster $n = 1$; $F = 1.0$ V Å^{-1}; $T = 230$ K. (i) Field ion micrograph of clean Pt tip in Ne at 3.75 V Å^{-1} provided for reference.

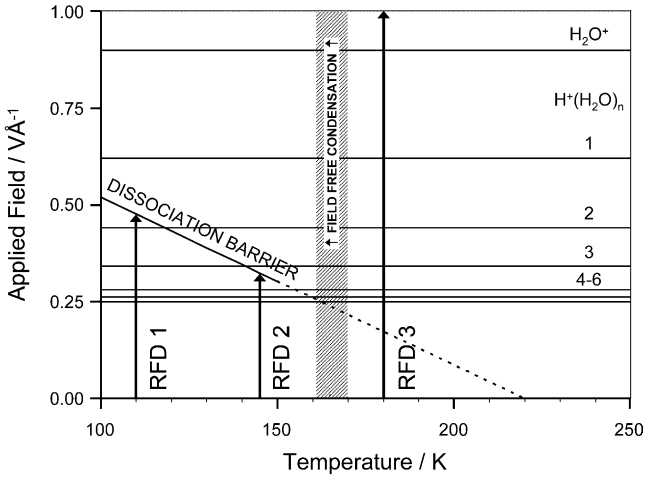

Fig. 5. A comparison of three RFDs. RFD1 is at 109 K and passes through the emission barriers for all clusters 2 and above and then reaches the dissociation barrier. RFD2 is at 145 K and passes through emission barriers for clusters above 3 before reaching the dissociation barrier. RFD3 is above the field-free condensation zone. It passes through the dissociation barrier prior to reaching any of the emission barriers. The emission barriers are taken from Rothfuss et al. [26]. The dissociation barrier is taken from Scovell et al. [24].

passes through each cluster $n = 4$ and above, prior to reaching the dissociation threshold. At the threshold, the ion clusters are again removed in a flash, but in this case $n = 2$ is not observed and only trace $n = 3$ ions are present, as observed in Fig. 3b. Finally, for RFD3 (180 K), the field ramp passes through the dissociation barrier prior to any of the emission barriers, resulting in dissociative ionization on the tip surface without ion emission. Ion emission begins only after the ramp reaches the high mass cluster emission fields and then favors each cluster type in turn moving to smaller clusters at higher fields (Fig. 1c).

4.2. Direct imaging of water ion cluster formation

To better understand the dynamics of the ion cluster formation, the full ion signal was imaged directly onto the MCPs at potentials corresponding to peak ion signals. The direct imaging of the ion formation in Fig. 4 clearly shows that the ionization/emission events are strongly localized for dissociated ionization. The higher mass clusters have fewer active locations. As the

field is increased, the dominant cluster size n decreases. With this decrease comes smaller and more numerous emission localities. Particular localities are temporary, but have extremely long lifetimes relative to the time scale of an ionization event. All pure white localities depicted lasted more than 10 s. Consequently, there must be a self-sustaining process that increases the probability of an emission event in an area where a previous event has occurred.

The results of these imaging experiments are consistent with a hump formation hypothesis. Ion emission occurs from localized points on the emitter surface for times that are epic relative to the timescale of an ionization event. A comparison of Fig. 4a–h with Fig. 4i does not suggest any correlation between surface geometry and emission localization, although such a correlation would be reasonable. From micrograph to micrograph, the positions of the localizations change. They were also observed to change on a time scale of about 20–30 s. However, it is possible that the state of the surface affects the emission event in a manner that is not obvious from analyzing the field cleaned image.

An effect similar to hump formation and localization of ion current is observed in the formation of Taylor cones [36] for liquid metal ion sources where the balance of surface tension and electrostatic pressure results in self-sustained ion sources with substantially enhanced electric fields. However, the enhanced field near the hump in the adsorbed water layer not only eases ion emission, but also increases the probability of dissociative ionization of additional water molecules near the hump. Consequently, the initial localization of charge results in a self-sustaining ionization and emission point. At low fields and temperatures, if the emission current is limited by the rate of dissociation, this enhancement would play an even more important role as both the supply of ions and the emission event are amplified.

4.3. The importance of solvation

Solvation of the proton (and hydroxyl ion) plays an important role in both dissociation of the water molecule and emission of the ion cluster. Fig. 6a shows an illustration of field induced ion dissociation in a thin water layer. The field is highest at the interfaces (Pt–water or water–vacuum) and is largely screened within the water layer [22]. However, dissociative ionization will not readily occur at either interface due to the lack of solvating water molecules. The dissociative event needs other water molecules to screen the charge and allow for separation of the proton from the hydroxyl ion. The degree of screening determines the energy barrier height for the dissociation, as well as the energies of the dissociation products after dissociation. If the barrier is too high, reaction will not proceed. The suitability of the local environment for accepting the dissociation products near a potential event plays a significant role in the dissociation step. The key to this suitability is the solvation of the dissociation products. Therefore, since the ionization event cannot readily occur at either interface due to solvation limitations, it will occur immediately inside either interface, where solvation is sufficient and the field remains high. The field at these locations will be much lower than the applied field on the tip.

After dissociation, the hydroxyl ion will move to the tip and discharge as shown between in Fig. 6b and c. The proton will remain on the tip until the field is sufficient to emit the ion cluster. While it resides on the tip, the solvating water molecules will help to screen the proton charge. However, the proton still represents a charge localization on the surface. This localization will attract other water molecules on the surface (through dipolar attraction) and result in further solvation of the proton. Eventually there will be a balance between the solvation rate and the desorption rate of the least bound solvating water molecules. Our earlier work [26] showed that the extent of solvation due to this balance is temperature dependent and effectively determines the largest available cluster for ion emission.

4.4. Water ion cluster field emission mechanism

The importance of the proton solvation shell continues through the emission event. Fig. 6b and c illustrate an idealized ion emission event. The ion emission event will not occur by simultaneously breaking all of the bonds with the surface. As the ion cluster pulls away, nearby water molecules are pulled towards the localized charge, forming a hump as the ion is emitted. The remaining water molecules are left in a state highly conducive to further dissociation events. First of all, there is a high local concentration of water providing an environment for proton/hydroxyl solvation. As the emission event occurs, the surface adsorbed water is pulled away from the tip resulting in a higher local thickness of the adlayer. This thicker layer provides an opportunity for three dimensional solvation, allowing for the dissociation event to occur *beneath* the surface of the water layer, as described above. Secondly, this hump formation leads to a high degree of local surface curvature. As a result, the field at the hump is enhanced. This may be compounded by the fact that the remaining local water molecules had adjusted their orientations to screen the charge of the nearby proton, resulting in a charge 'vacancy' after the ion emission event has occurred.

4.5. Notes on low temperature cluster formation

The picture presented of the two step mechanism so far has focused on the dissociation and emission events,

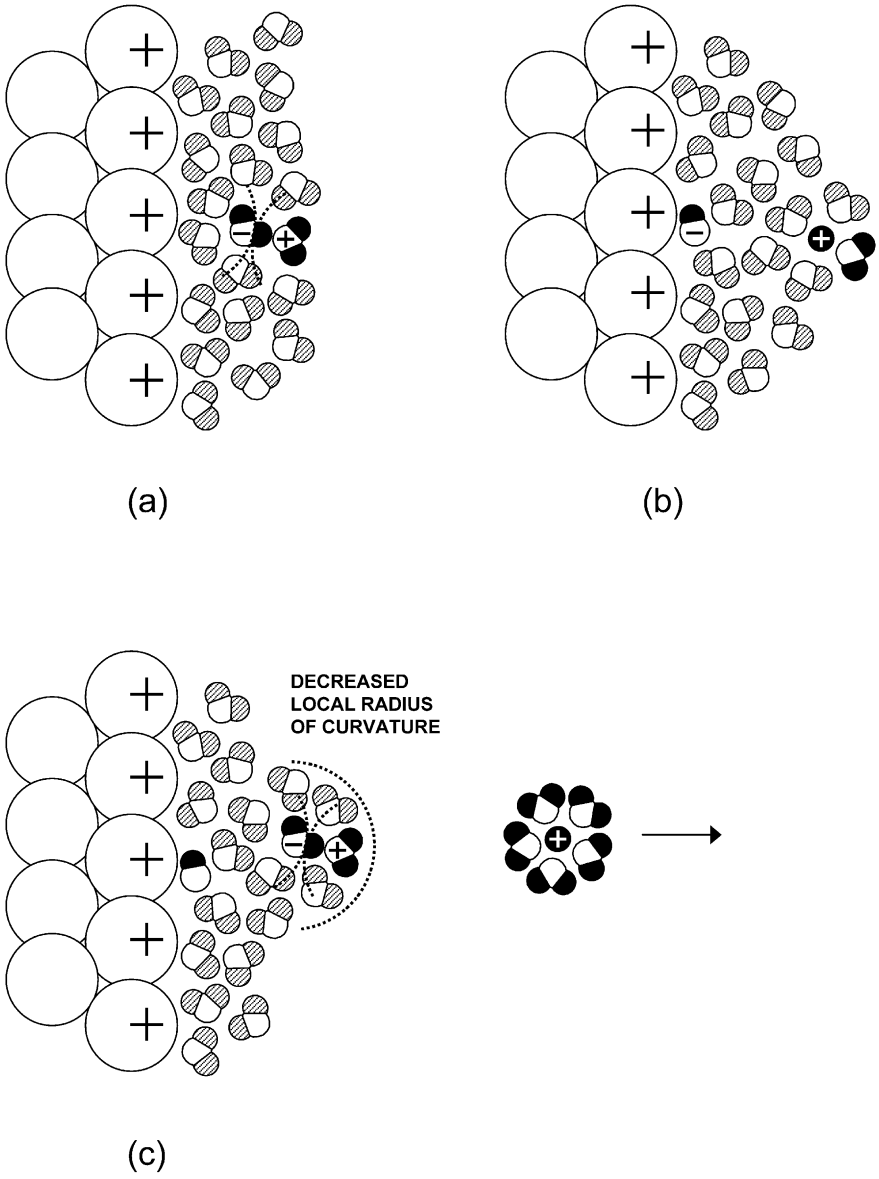

Fig. 6. Idealized model of 2 step ionization/emission mechanism. (a) Water molecule in field begins to dissociate. Dissociation probability is influenced by the alignment of molecules and the extent of local solvation for accepting. (b) After dissociation, the hydroxyl moves to the tip surface to discharge and the solvated proton moves to the vacuum interface for emission if the field is strong enough. (c) After emission, a localization is created with a decreased local radius of curvature. This localization provides a higher local probability of dissociation due to field enhancement.

without consideration of transport phenomena. In the field-adsorbed water layer experiments, there is a high incident flux and low residence time of water on the surface, and surface diffusion occurs relatively freely, allowing transport to be largely neglected. However, for the ice deposition RFD experiments, the solvation, cluster formation and emission events are complicated by transport limitations. The onset of surface diffusion near 130 K may be responsible for the slope break in emission onset observed by Scovell et al. [24] (Fig. 2a). This mobility would provide a greater capacity for solvating the proton during dissociation near the surface (where the field is strongest). Near 150 K, molecular transport within bulk ice becomes possible, which may further facilitate dissociation; however RFD experiments at this temperature have not been carried out. The limitation of transport of water molecules is not the only significant consequence of the low temperature. Hydroxyl transfer through the ice layer (most likely by proton hopping) to discharge at the tip surface may also be transport limited. If the hydroxyl discharge cannot occur quickly, there will be a negative charge buildup near the water surface, effectively screening the tip field and shutting down emission.

4.6. Reconsidering previous investigations

The two step ion dissociation and emission mechanism outlined in this discussion provides a framework for explaining observations in previous literature concerning ion cluster emission from emitter tips. In Anway's discussion [18] of the field-ionization of water, he suggested an adlayer with 'long whiskers of water molecules oriented dipole to dipole' extending out from the tip surface. This provided an explanation of how large clusters could be emitted in a single ionization event, and was consistent with his experimental observations. Significant work by Block's group [37–39] on field assisted photodesorption of water (and other molecules) from emitter tips was carried out that supported the whisker model. However, there were some suggestions among their results that the whisker model was incomplete. The two step mechanism appears to address these concerns.

The experiments performed by Block and coworkers [37,38] were carried out at low temperature (80 K) with ice layers deposited in the presence of a field, and a continuous background pressure of water. Molecules were ionized by synchrotron radiation (~ 175 nm) in the presence of an applied field. Looking back on their research in the light of the present results suggests that the effective fields were above the desorption barrier for all cluster types, but below the dissociation barrier. The synchrotron radiation provided sufficient energy (and more) for the dissociation event to occur, and then the field was sufficient for cluster emission. Among their observations are several that should be revisited with consideration of a two step mechanism.

Block and coworkers found that with no field present, only protons were emitted from the surface, while at an applied field of 1 V $Å^{-1}$, protonated water clusters with n up to 16 were observed. While this is consistent with a whisker model, it is also consistent with the two step mechanism. In the absence of a field, protons formed by the dissociating radiation lack further energy for emission from the surface. Block and coworkers suggest that emission of protons is simply due to photon stimulated dissociation of surface molecules, which is reasonable. Under field conditions, the whisker model contends that one of the whisker constituents is ionized by the synchrotron radiation, essentially snipping off the whisker at the point of ionization. This provides an explanation for the formation of large clusters in general, but there are a number of areas where it falls short. In particular, there is no way of accounting for the observed ion cluster distributions. In fact they found it [38] 'remarkable that under these conditions almost no monomers and very few dimers were detected.' Based on the whisker model, it is reasonable to assume that in every situation the monomer and dimer would dominate. This is due to the fact that every n length whisker contains the set of all smaller cluster types. There is no obvious reason why photo-ionization would occur preferentially towards the base of the whisker, so monomers and dimers would be expected in a single step process that does not account for solvation energies. However, in the two step mechanism, ionization and emission are temporally separated and both strongly influenced by solvation. These photon assisted desorption experiments are analogous to low temperature RFD experiments, but instead of ramping up to the dissociation barrier, the field is stabilized just below the barrier, and then individual molecules are kicked over it with the radiation.

Dirks et al. [39] extended this work to include a study of the effect of temperature variation (80–140 K). They observed that the cluster size distribution varied with temperature, favoring larger clusters at higher temperatures, which they attributed to the increase in 'translational transport'. While the translational transport may be able to explain an increase in the higher mass clusters, it does not explain the complete absence of $H^+(H_2O)$ and $H^+(H_2O)_2$ clusters in their 120 and 140 K spectra. However, Fig. 5 suggests that at these temperatures, the dissociation barrier is below the emission barrier for $H^+(H_2O)$ and $H^+(H_2O)_2$ clusters, so with the two step mechanism, the surprising lack of low mass clusters is actually expected.

The two step mechanism nicely explains the Block group observations, but it was largely Anway's energy deficit data [18] that led to the acceptance of the whisker hypothesis. The whisker model allowed for ions to form at variable distances from the emitter tip, providing an explanation for the observed energy deficit data. The hump formation and ion dissociation localization effect provides the same three dimensional characteristics that Anway needed to explain his energy deficits, providing consistency with this earlier work as well.

More recently, Stintz and Panitz [19–21] performed experiments on water ion cluster formation from deposited ice layers on emitter tips. For these experiments the water was deposited under field-free conditions and the field was ramped (at a variety of temperatures) to induce ion emission. Their observations included an increased ionization onset field at lower temperatures and a corresponding change in ion cluster distribution consistent with our low temperature work. An examination of these results shows them to be consistent with our proposed mechanism.

The proposed mechanism for field induced dissociation and emission of water molecules is capable of explaining the experimental observations discussed in the prior literature, and overcoming the shortfalls of the previous whisker model. This suggests that field adsorbed water layers are even better analogs of the electrochemical double layer than previously thought. Screening and solvation effects are critical to the

behavior of the double layer. Under conditions where the behavior of the field adsorbed layer is dominated by solvation and charge screening, the emitter tip provides an excellent test bed for studying these phenomena.

5. Conclusions

The emission of ions from a field emitter tip has traditionally been thought of as a single event process where the ionization and emission were assumed to occur nearly simultaneously. Our research into the field induced ion emission of protonated water clusters from both deposited ice layers and field adsorbed water layers suggests otherwise. The evidence supports a two-step mechanism requiring first the dissociation of an adsorbed molecule followed later by ion emission. The energy barriers for these steps are distinct and are influenced differently by the applied field. The situation is further complicated by the temperature dependence of solvation of the proton on the surface and the availability of solvating water molecules.

Based on the results of the field adsorbed water ionization and ice deposition RFDs, two independent steps are required for water ion cluster emission. The first step, water dissociation, is a field-enhanced, thermally activated process with an activation energy of $\sim$ 0.7 eV. The extent of solvation of the product ion pair ($H^+ \ldots OH^-$) is important to the success of the dissociation event. After the water molecule dissociates, the OH^- discharges on the tip and the proton remains in an intermediate state on the surface, solvated by nearby water molecules. These solvating water molecules are bound to the proton by their solvation energies. The extent of solvation depends on the tip temperature, as desorption of the solvating molecules is thermally activated, requiring more energy with decreasing n. The extent of solvation determines the minimum field required for the second step, ion emission. If the field is sufficient, ion emission occurs. The emission event acts to facilitate additional dissociation events locally and an emission localization occurs.

Acknowledgements

This research was made possible through funding by the Office of Naval Research. Video imaging and processing was performed in part using freely distributable GPL software from virtualdub.org. EMS gratefully acknowledges two decades of lively scientific interchanges and uproariously funny moments with a fellow rider of the rails, Mike Weaver.

References

[1] D. Price, J.W. Halley, J. Electroanal. Chem. 159 (1983) 347.
[2] J. Kreuzer, Surf. Sci. 246 (1991) 336.
[3] W. Schmickler, Surf. Sci. 335 (1995) 416.
[4] J.K. Sass, Vacuum 33 (1983) 741.
[5] E.M. Stuve, N. Kizhakevariam, J. Vac. Sci. Technol. A 11 (1993) 2217.
[6] K. Bange, B. Straehler, J.K. Sass, R. Parsons, J. Electroanal. Chem. 229 (1987) 87.
[7] J.K. Sass, K. Kretzxchmar, S. Holloway, Vacuum 31 (1981) 483.
[8] E.M. Stuve, A. Krasnopoler, D.E. Sauer, Surf. Sci. 335 (1995) 177.
[9] M.J. Weaver, N. Kishakevariam, X. Jiang, J. Chem. Phys. 100 (1994) 6750.
[10] I. Villegas, M.J. Weaver, J. Phys. Chem. 101 (1997) 5842.
[11] M.J. Weaver, S. Zou, C. Tang, J. Chem. Phys. 111 (1999) 368.
[12] M.J. Weaver, S.A. Wasileski, Langmuir 17 (2000) 3039.
[13] S.A. Wasileski, M.T.M. Koper, M.J. Weaver, J. Chem. Phys. 115 (2001) 8193.
[14] S.A. Wasileski, M.T.M. Koper, M.J. Weaver, J. Am. Chem. Soc. 124 (2002) 2796.
[15] M.G. Inghram, R. Gomer, Z. Naturforschg 10a (1955) 863.
[16] H.D. Beckey, Principles of Field Ionization and Field Desorption Mass Spectrometry, Pergamon Press, Oxford, 1977.
[17] W.A. Schmidt, Z. Naturforschg 19a (1964) 318.
[18] A.R. Anway, J. Chem. Phys. 50 (1969) 2012.
[19] A. Stintz, J.A. Panitz, J. Appl. Phys. 72 (1992) 741.
[20] A. Stintz, J.A. Panitz, Surf. Sci. 296 (1993) 75.
[21] A. Stintz, J.A. Panitz, Int. J. Mass Spectrometry Ion Processes 133 (1994) 59.
[22] D.L. Scovell, T.D. Pinkerton, B.A. Finlayson, E.M. Stuve, Chem. Phys. Lett. 294 (1998) 255.
[23] D.L. Scovell, T.D. Pinkerton, V.K. Medvedev, E.M. Stuve, Proc. Electrochem. Soc. 5 (1999) 6.
[24] D.L. Scovell, T.D. Pinkteron, V.K. Medvedev, E.M. Stuve, Surf. Sci. 457 (2000) 365.
[25] T.D. Pinkerton, D.L. Scovell, A.L. Johnson, B. Xia, V. Medvedev, E.M. Stuve, Langmuir 15 (1999) 851.
[26] C.J. Rothfuss, V.K. Medvedev, E.M. Stuve, Surf. Sci. 501 (2002) 169.
[27] P.L. Geissler, C. Dellago, D. Chandler, J. Hutter, M. Parrinello, Science 291 (2001) 2121.
[28] L.A. Montero, J. Molina, J. Fabian, Int. J. Quantum Chem. 79 (2000) 8.
[29] J.A. Mejias, S. Lago, J. Chem. Phys. 113 (2000) 7306.
[30] M.F. Kropman, H.J. Bakker, Science 291 (2001) 2118.
[31] E.R. Batista, S.S. Xantheas, H. Johnnson, J. Chem. Phys. 112 (2000) 3285.
[32] T.D. Pinkerton, D.L. Scovell, A.L. Johnson, B. Xia, V.K. Medvedev, E.M. Stuve, Langmuir 15 (1999) 851.
[33] T.T. Tsong, Atom-Probe Field Ion Microscopy—Field Ion Emission and Surface and Interfaces at Atomic Resolution, Cambridge University Press, Cambridge, 1990.
[34] G.F. Rempfer, J. Appl. Phys. 57 (1985) 385.
[35] P.V. Hobbs, Ice Physics, Oxford University Press, London, 1974.
[36] G. Taylor, Proc. Roy. Soc. Lond. A 280 (1964) 383.
[37] S. Jaenicke, A. Ciszewski, W. Drachsel, U. Weigmann, T.T. Tsong, J.R. Pitts, J.H. Block, D. Menzel, J. De Physique 47 (1986) 343.
[38] S. Jaenicke, A. Ciszewski, J. Doesselmann, W. Drachsel, J.H. Block, D. Menzel, J. De Physique 49 (1988) 191.
[39] J. Dirks, W. Drachsel, J.H. Block, J. De Physique 50 (1989) 153.